



Physicochemical studies of green phosphorescent light-emitting materials from cyclometalated heteroleptic iridium(III) complexes

Jayaraman Jayabharathi*, Venugopal Thanikachalam, Natesan Srinivasan, Marimuthu Venkatesh Perumal

Department of Chemistry, Annamalai University, Annamalai Nagar 608 002, Tamil Nadu, India

ARTICLE INFO

Article history:

Received 28 January 2011

Received in revised form 19 February 2011

Accepted 25 February 2011

Keywords:

Green emitters

HOMO–LUMO

ΔQ_e

Energy gap law

Quantum efficiency

ABSTRACT

A series of novel imidazole ligands were synthesized and characterized. Phosphorescence studies of series of heteroleptic cyclometalated iridium(III) complexes reveal that these complexes possess dominantly $^3\text{MLCT}$ and $^3\pi-\pi^*$ excited states and the solvent shifts of these complexes are interpreted by Richardt–Dimroth and Marcus solvent functions. The results consistent with prior assignments on the absorption band to a metal-to-ligand charge transfer excited state associated with chelating ligand. Emission kinetic studies exploited that the radiative transition (k_r), increases with increasing λ_{em} and linear correlation exists between $\ln(k_{\text{nr}})$ and energy gap. Electronic transition theory is applied to study the effect of E_g and ΔQ_e on non-radiative transition (k_{nr}). With a larger ΔQ_e , favouring vibrational overlap and leading to a larger value for k_{nr} .

© 2011 Elsevier B.V. All rights reserved.

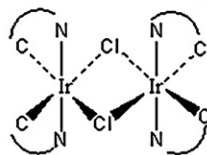
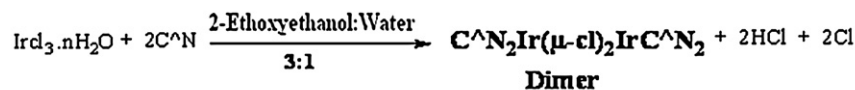
1. Introduction

Electrophosphorescent materials incorporating complexes of heavy metals have been aroused particularly attention in last decade due to their extremely high efficiency as electroluminescent emitters. They mainly include square planar d^8 or octahedral d^6 complexes of heavy-metals such as Pt(II), Ru(II), Os(II), and Ir(III) [1–6]. Of these materials, iridium complexes have been regarded as the most appropriate phosphorescent materials because of their relatively short lifetime and high quantum efficiency. These Ir complexes generally contain two cyclometalated ligands ($\text{C}\hat{\text{N}}$) and a single bidentate, monoanionic ancillary ligand, or with three cyclometalated ligands. The cyclometalated ligands used in the complexes are well known as heterocycle derivatives that coordinated to the metal center via formation of Ir–N and Ir–C bonds. Therefore, design of ligands for Ir complexes is of great importance in order to achieve high efficiency and color purity for organic light emitting diodes (OLEDs). To date, most researches were focused on the design and synthesis of the cyclometalated ligand, such as changing π conjugation, introducing electron donating or withdrawing group on the appropriate position of the aromatic ring [7–10], and adopting rigid structure.

Tuning phosphorescence wavelength and enhancing phosphorescent quantum yield in these complexes is attractive for both fundamental research and practical applications [11–20]. Our ongoing investigation [18–21] of phosphorescent imidazole based cyclometalated iridium(III) complexes ($\text{C}\hat{\text{N}}_2\text{Ir}(\text{LX})$), we have observed that electron releasing substituent on the imidazole ligands have a remarkable influence on the electrochemical and photophysical properties. These complexes show unusual high HOMO (highest occupied molecular orbital) levels and exhibit exceedingly high efficiency even at relatively low dopant concentration. Our interest in the development of highly efficient phosphors for applications in OLEDs prompted us to synthesize heteroleptic iridium complexes and investigate their photophysical properties. In the present study the methyl group as electron releasing moiety was chosen due to the emissions of iridium complex come from phosphorescence with triplet character of both ligand centered ($\pi-\pi^*$) and MLCT (metal-to-ligand charge transfer) transitions. The phosphorescence is strongly affected by the triplet energy of the *ortho*-chelating $\text{C}\hat{\text{N}}$ ligands. Therefore substituents, even methyl groups could play a key role in the alteration of the triplet energy and although a methyl group is a weaker electron donating group than other functional groups (e.g. $-\text{OCH}_3$, NR_2 , etc.). Incorporating a methyl group as a substituent on the imidazole ring has an influence on the HOMO/LUMO level (lowest unoccupied molecular orbital), as well as $^3\text{MLCT}$ state of the complex. Herein we described the results of our systematic investigation on the preparation, structural characterization, photophysical properties and electrochemical behaviour of cyclometalated iridium complexes.

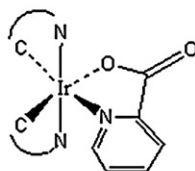
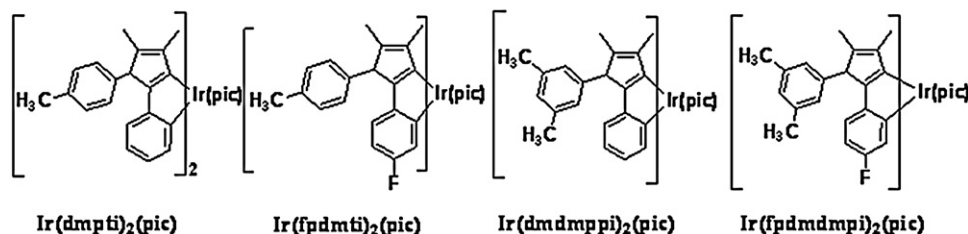
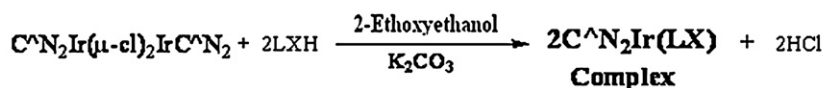
* Corresponding author. Tel.: +91 4144 239523; mobile: +91 9443940735.
E-mail address: jtchalam2005@yahoo.co.in (J. Jayabharathi).

Synthesis of Dimer



Coordination geometry of the chloride bridged dimer

Synthesis of Heterolyptic Iridium Complex



Coordination geometry of the $(\text{C}^{\wedge}\text{N})_2\text{Ir}(\text{acac})$ complex

Scheme 1. Synthesis of iridium complexes $(\text{C}^{\wedge}\text{N})_2\text{Ir}(\text{acac})$ 1–4.

2. Experimental

2.1. Materials and methods

Iridium(III)trichloride trihydrate ($\text{IrCl}_3 \cdot 3\text{H}_2\text{O}$, Sigma–Aldrich Ltd.), 2-ethoxyethanol ($\text{H}_5\text{C}_2\text{OC}_2\text{H}_4\text{OH}$, S.D. fine) and all other reagents used without further purification.

2.2. Optical measurements and compositions analysis

The ultraviolet–visible (UV–vis) spectra of the phosphorescent Ir(III) complexes were measured in an UV–vis spectrophotometer (Perkin Elmer Lambda 35) and corrected for background absorption due to solvent. Photoluminescence (PL) spectra were recorded on a (Perkin Elmer LS55) fluorescence spectrometer. The solid-state emission spectra were recorded on fluoromax2 (ISA SPEX) Xenon-Arc lamp as a source. NMR spectra were recorded on a Bruker 400 MHz NMR spectrometer. MS spectra (Fast Atom Bombardment) were recorded on a Varian Saturn 2200 GC–MS spectrometer. Cyclic Voltammetry (CV) analyses were performed by using CHI 630A potentiostat electrochemical analyzer. Measurements of oxidation and reduction were undertaken using 0.1 M tetra(*n*-butyl)ammoniumhexafluorophosphate as a supporting electrolyte,

at scan rate of 0.1Vs^{-1} . The potentials were measured against an Ag/Ag^+ (AgCl) reference electrode using ferrocene/ferrocenium ($\text{Cp}_2\text{Fe}/\text{Cp}_2\text{Fe}^+$) as the internal standard. The onset potentials were determined from the intersection of two tangents drawn at the rising current and background current of the cyclic voltammogram.

2.3. General procedure for the synthesis of ligands

The various substituted 2-arylimidazole ligands were prepared from an unusual four components assembling of butan-2,3-dione, ammonium acetate, methyl substituted aryl amine and substituted aryl aldehyde [18–21].

2.3.1. 4,5-dimethyl-2-phenyl-1-*p*-tolyl-1*H*-imidazole (dmpti)

Yield: 48%. ^1H NMR (400 MHz, CDCl_3): δ 2.42 (s, 3H), 2.31 (s, 3H), 2.02 (s, 3H), 7.02–7.36 (aromatic protons). ^{13}C NMR (100 MHz, CDCl_3): δ 9.57, 12.76, 21.19, 125.45, 127.54, 127.63, 127.97, 128.01, 130.11, 130.92, 133.41, 135.34, 138.37, 145.15. Anal. calcd. for $\text{C}_{18}\text{H}_{18}\text{N}_2$: C, 82.41; H, 6.92; N, 10.68. Found: C, 82.12; H, 6.02; N, 10.08. MS: m/z 262.15, calcd. 262.00.

2.3.2. 2-(4-Fluorophenyl)-4,5-dimethyl-1-p-tolyl-1H-imidazole (fpdmti)

Yield: 40%. $^1\text{H NMR}$ (400 MHz, CDCl_3): δ 2.01 (s, 3H), 2.29 (s, 3H), 2.43 (s, 3H), 6.87–7.34 (aromatic protons). $^{13}\text{C NMR}$ (100 MHz, CDCl_3): δ 9.53, 12.69, 21.18, 114.92, 115.10, 125.44, 127.16, 129.89, 130.20, 133.35, 135.13, 138.57, 144.28, 161.26, 163.23. Anal. calcd. for $\text{C}_{18}\text{H}_{17}\text{N}_2\text{F}$: C, 77.12; H, 6.11; N, 9.99. Found: C, 76.24; H, 5.98; N, 8.99. MS: m/z 280.00, calcd. 280.14.

2.3.3.

4,5-Dimethyl-1-(3,5-dimethylphenyl)-2-phenyl-1H-imidazole (dmdmppi)

Yield: 45%. $^1\text{H NMR}$ (400 MHz, CDCl_3): δ 1.98 (s, 3H), 2.27 (s, 3H), 2.29 (s, 6H), 6.77–7.36 (aromatic protons). $^{13}\text{C NMR}$ (100 MHz, CDCl_3): δ 9.65, 12.77, 21.27, 125.54, 125.59, 127.59, 127.97, 128.03, 130.02, 130.07, 133.53, 137.88, 139.33, 144.98. Anal. calcd. for $\text{C}_{19}\text{H}_{20}\text{N}_2$: C, 82.57; H, 7.29; N, 10.14. Found: C, 82.01; H, 6.89; N, 9.12. MS: m/z 276.00, calcd. 276.16.

2.3.4. 2-(4-Fluorophenyl)-4,5-dimethyl-1-(3,5-dimethylphenyl)-1H-imidazole (fpdmdmpi)

Yield: 45%. $^1\text{H NMR}$ (400 MHz, CDCl_3): δ 1.99 (s, 3H), 2.27 (s, 3H), 2.31 (s, 6H), 6.77–7.34 (aromatic protons). $^{13}\text{C NMR}$ (100 MHz, CDCl_3): δ 9.5, 12.69, 21.15, 114.81–163.41 (aromatic carbons). Anal. calcd. for $\text{C}_{19}\text{H}_{19}\text{N}_2\text{F}$: C, 77.52; H, 6.51; N, 9.52. Found: C, 77.01; H, 6.02; N, 9.21. MS: 294.00, calcd. 294.15.

2.4. General procedure for the synthesis of iridium complexes (1–4)

The 2-aryl imidazole based cyclometalated iridium complexes **1–4** were synthesized from $\text{IrCl}_3 \cdot 3\text{H}_2\text{O}$ and the 2-aryl imidazole ligands to give the corresponding dimeric species via the Nonoyama route [22] followed by the treatment with picolinic acid in the presence of K_2CO_3 as shown in Scheme 1.

2.4.1. Iridium(III)bis(4,5-dimethyl-1-(p-methylphenyl)-2-phenyl-1H-imidazolato-N,C2')(picolanate), Ir(dmpti)(pic), **1**

Yield: 65%. $^1\text{H NMR}$ (400 MHz, CDCl_3): δ 1.28 (s, 6H), 1.96 (s, 6H), 2.20 (s, 3H), 2.50 (s, 3H), 6.01–8.04 (aromatic protons). $^{13}\text{C NMR}$ (100 MHz, CDCl_3): δ 9.12, 9.16, 9.21, 10.25, 22.69, 119.50, 120.36, 122.10, 124.17, 127.20–136.42, 139.83, 146.89, 149.36, 156.20, 157.36. Anal. calcd. for $\text{C}_{42}\text{H}_{38}\text{IrN}_5\text{O}_2$: C, 60.27; H, 4.58; N, 8.37. Found: C, 60.13; H, 4.46; N, 8.16. MS: m/z 837.27, calcd. 836.69.

2.4.2. Iridium(III)bis(4,5-dimethyl-1-(p-methylphenyl)-2-fluorophenyl-1H-imidazolato-N,C2')(picolanate), Ir(fpdmti)(pic), **2**

Yield: 65%. $^1\text{H NMR}$ (400 MHz, CDCl_3): δ 1.28 (s, 3H), 1.32 (s, 3H), 1.89 (s, 3H), 1.93 (s, 3H), 2.17 (s, 3H), 2.51 (d, 3H), 2.53 (s, 3H), 7.23 (m, 3H), 7.29 (m, 1H), 7.40 (m, 5H), 7.89 (m, 2H), 8.30 (m, 1H), 6.07 (dd, 1H), 6.22 (m, 4H), 6.38 (dd, 1H). $^{13}\text{C NMR}$ (100 MHz, CDCl_3): δ 9.13, 9.19, 10.16, 21.35, 119.46, 120.16, 123.31, 124.35, 127.33, 127.83, 128.16, 128.27, 130.56, 130.98, 132.53, 133.31, 133.41, 136.85, 139.89, 140.10, 149.27, 153.17, 155.37, 156.53, 160.93, 162.87. Anal. calcd. for $\text{C}_{42}\text{H}_{36}\text{IrF}_2\text{N}_5\text{O}_2$: C, 57.78; H, 4.16; N, 8.02. Found: C, 56.93; H, 4.03; N, 7.93. MS: m/z 873.25, calcd. 872.69.

2.4.3. Iridium(III)bis(4,5-dimethyl-1-(3,5-dimethylphenyl)-2-phenyl-1H-imidazolato-N,C2')(picolanate), Ir(dmdmppi)(pic), **3**

Yield: 65%. $^1\text{H NMR}$ (400 MHz, CDCl_3): δ 1.28 (s, 3H), 1.35 (s, 3H), 1.95 (s, 3H), 1.92 (s, 3H), 2.20 (s, 3H), 2.43 (d, 3H), 2.38 (d, 3H), 6.20–8.32 (aromatic protons). $^{13}\text{C NMR}$ (100 MHz, CDCl_3): δ 9.12,

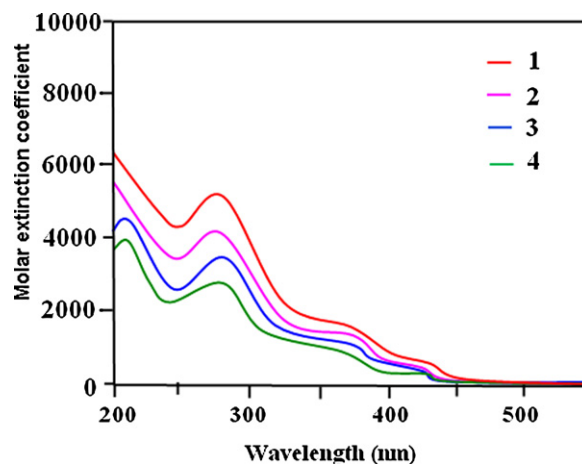


Fig. 1. The UV-vis absorption spectra of the complexes **1–4** in CH_2Cl_2 .

9.22, 10.23, 21.25, 29.70, 119.49, 120.37, 122.14, 124.30, 125.97, 127.10–127.42, 131.29, 133.24, 134.09, 136.36, 140.08, 144.73, 149.38, 153.41, 156.05, 157.28. Anal. calcd. for $\text{C}_{44}\text{H}_{42}\text{IrN}_5\text{O}_2$: C, 61.09; H, 4.89; N, 8.10. Found: C, 60.89; H, 4.53; N, 8.01. MS: m/z 865.30, calcd. 864.29.

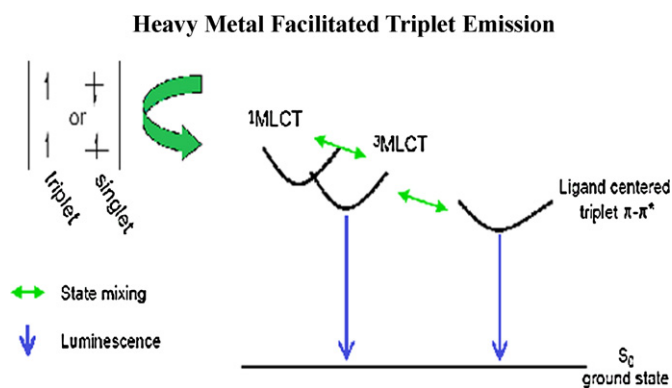
2.4.4. Iridium(III)bis(4,5-dimethyl-1-(3,5-dimethylphenyl)-2-fluorophenyl-1H-imidazolato-N,C2')(picolanate), Ir(fpdmdmpi)(pic), **4**

Yield: 65%. $^1\text{H NMR}$ (400 MHz, CDCl_3): δ 1.32 (s, 3H), 1.93 (d, 6H), 2.18 (s, 3H), 2.40 (s, 6H), 2.44 (d, 6H), 6.07–8.04 (aromatic protons). $^{13}\text{C NMR}$ (100 MHz, CDCl_3): δ 9.20, 10.15, 21.18, 29.70, 119.29, 120.16, 123.45, 124.25, 125.26–127.39, 131.33, 132.38–140.35, 149.29, 153.23, 155.21, 156.43, 160.92, 162.90. Anal. calcd. for $\text{C}_{44}\text{H}_{40}\text{IrN}_5\text{F}_2\text{O}_2$: C, 58.65; H, 4.47; N, 7.77. Found: C, 58.37; H, 4.36; N, 7.12. MS: m/z 901.28, calcd. 900.79.

3. Results and discussion

3.1. Photophysical properties

The absorption bands of the series of complexes (**1–4**) show two kinds of bands (Fig. 1). The intense bands observed around 270 nm in the ultraviolet part of the spectrum can be assigned to the allowed ligand centered ($\pi\text{--}\pi^*$) transitions [23] and somewhat weaker bands also observed in the lower part of energy ($\lambda_{\text{max}} < 370$ nm). The band position, size and extinction coefficient of the bands observed in the range 370–447 nm suggest that these are MLCT transitions ($^1\text{MLCT}$ and $^3\text{MLCT}$) [24,25]. According to our previous papers [18–21], weak bands located at longer wavelength have been assigned to the $^1\text{MLCT} \leftarrow S_0$ and $^3\text{MLCT} \leftarrow S_0$ transitions of iridium complexes. Thus the broad absorption shoulders at 386 and 438 nm observed for **1** are likely to be ascribed to the $^1\text{MLCT} \leftarrow S_0$ and $^3\text{MLCT} \leftarrow S_0$ transitions, respectively. The intensity of the $^3\text{MLCT} \leftarrow S_0$ transition is close to that of $^1\text{MLCT} \leftarrow S_0$ transition, suggesting that $^3\text{MLCT} \leftarrow S_0$ transition is strongly allowed by S–T mixing of spin–orbit coupling [12] and similar observations are made for other complexes **2–4**. Absorption in the range of around 370 nm for complexes (**1–4**) corresponds to the transition of the $^1\text{MLCT}$ state as evident from its extinction coefficient of the order 10^3 . The absorption like long tail toward lower energy and higher wavelength around 428 nm is assigned to $^3\text{MLCT}$ transitions and gains intensity by mixing with the higher lying $^1\text{MLCT}$ transitions through the spin–orbit coupling (Fig. 2) of iridium(III) [17]. Both singlet MLCT ($^1\text{MLCT}$) and triplet MLCT ($^3\text{MLCT}$) bands are typically observed for these complexes in all solvents. In order for these



iridium (III) complexes to be useful as phosphors EL devices, strong spin-orbit coupling must be present to efficiently mix the singlet and triplet excited states. Clear evidences for mixing of the singlet and triplet excited states are seen in the absorption (Fig. 1) of these complexes.

3.2. Phosphorescence spectra

3.2.1. Mixing of excited states (LC and MLCT)

Phosphorescence of mononuclear metal complexes originates from the ligand-centered excited state, metal-centered excited state and MLCT excited state. For the cyclometalated iridium(III) complexes, the wave function of the excited triplet state Φ_T , responsible for the phosphorescence is expressed as,

$$\Phi_T = a \Phi_T(\pi - \pi^*) + b \Phi_T(\text{MLCT}) \quad (1)$$

where 'a' and 'b' are the normalized co-efficients, $\Phi_T(\pi - \pi^*)$ and $\Phi_T(\text{MLCT})$ are the wave function of $^3(\pi - \pi^*)$ and $^3(\text{MLCT})$ excited states, respectively. For these iridium complexes, the wave function of the triplet state (Φ_T) responsible for the phosphorescence and Eq. (1) implies that the excited triplet state of these iridium complexes are mixture of $\Phi_T(\pi - \pi^*)$ and $\Phi_T(\text{MLCT})$ [26]. The triplet state is attributed to dominantly $^3\pi - \pi^*$ excited state when $a > b$ and dominantly $^3\text{MLCT}$ excited state when $b > a$.

The phosphorescence spectra of these complexes (1–4) obtained at 298 K show significant broad shape and also vibronic fine structure (Fig. 3). According to our previous studies [18–21], phosphorescence spectra from the ligand centered $^3\pi - \pi^*$ state display vibronic progressions, while those from the $^3\text{MLCT}$ state are broad

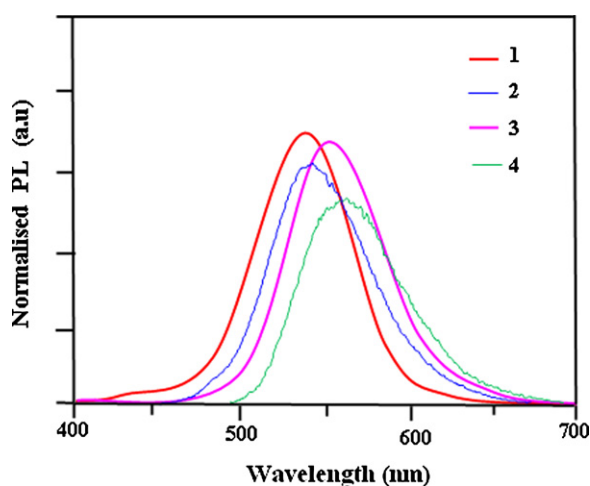


Fig. 3. The photoluminescence emission spectra of the complexes 1–4 in CH_2Cl_2 .

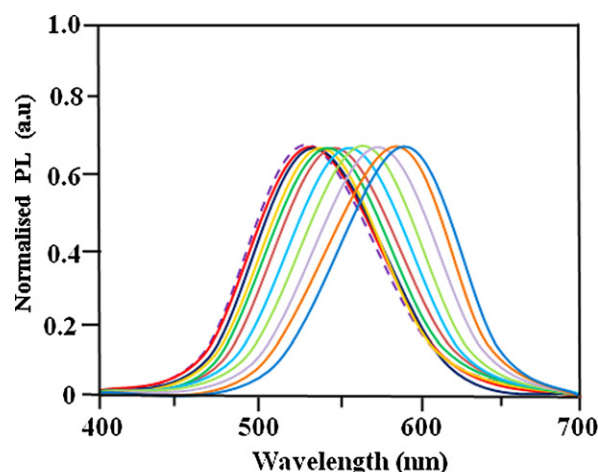


Fig. 4. The solid state and the solvatochromic emission spectra of complex 1.

in shape. The luminescence spectra of complexes 1 and 3 reveal broad shape of the luminescence spectra (Fig. 3) whereas the vibrational sideband pattern of the photoluminescence spectra were observed for the complexes 2 and 4 (Fig. 3). Complexes 1 and 3 have excited state with large contribution of $^3\text{MLCT}$ whereas complexes 2 and 4 have excited state with large contribution of $^3\pi - \pi^*$. All these complexes show emission at 540, 550, 553 and 560 nm in dichloromethane, respectively (Table 1). The emission spectra of complexes 1 and 3 are slightly blue-shifted in comparison with that of complexes 2 and 4. $[\text{Ir}(\text{dmpti})_2(\text{pic})]$ (1) is blue shifted in comparison with that of $[\text{Ir}(\text{dmdmppi})_2(\text{pic})]$ (3), which is the result of the introduction of electron withdrawing fluorine substituent into the phenyl ring attached to C(2) carbon of the imidazole ring in complexes 2 and 4. The Stokes shift (Table 1) of 1–4 was calculated in wave numbers from the difference between the lowest energy absorption maximum and the emission maximum of each complex. The observed large Stokes shift in hydroxyl solvents may be due to the significant structural differences between the ground state and excited state of these iridium complexes [28].

3.2.2. Marcus and Richardt–Dimroth solvent functions – solvatochromism

Solvatochromism is a potentially important probe in accessing charge distributions in both ground and excited states and also yield information regarding charge distributions in Franck–Condon states produced by absorption. Solvent shifts in the absorption and emission of *ortho*-metalated iridium complexes 1–4 were measured (Table 1) in different solvents. Variation in the absorption and emission of the complexes 1–4 was observed in different solvents. The representative emission spectra of complex $[\text{Ir}(\text{dmpti})_2(\text{pic})]$ 1 is shown in Fig. 4. The emission peak of complexes 1–4 are around 528 nm in *n*-hexane (non-polar), 570 nm in ethanol (polar protic solvent), 540 nm in CH_2Cl_2 (medium polarity) and 580 nm in acetonitrile (a strongly polar aprotic solvent). The peak shift may be due to the stronger interaction between the solvents and the excited state molecules. The excited state of all iridium complexes are more stabilized in polar solvents than in non-polar solvents which lead to red shift of emission with increasing solvent polarity [24] (Fig. 4). The photoluminescent peak of solid state (representative spectrum of complex 1 is shown in Fig. 4) of all complexes

Table 1
Photoluminescence spectral data of various solvents and solid emission spectra of complexes **1–4**.

Solvent	Absorption ^a (λ , nm) (log ϵ)				Emission ^b (λ , nm)				Stokes shift (cm^{-1})			
	1	2	3	4	1	2	3	4	1	2	3	4
<i>n</i> -Hexane	269.0 (3.785)	282.0 (3.982)	286.0 (3.883)	284.0 (3.973)	528	530	537	541	3892	4068	4634	4718
Benzene	386.0 (3.224)	379.0 (3.084)	380.0 (3.589)	382.0 (3.075)	530	532	538	544	4496	4622	4244	4553
	438.0 (2.268)	436.0 (2.363)	430.0 (2.408)	431.0 (2.369)								
1,4-dioxane	270.0 (3.956)	272.0 (3.794)	273.0 (3.775)	274.0 (3.857)	534	540	545	547	3645	4209	3973	3794
	375.0 (3.412)	370.0 (3.056)	378.0 (3.113)	380.0 (3.121)								
Chloroform	428.0 (2.284)	427.0 (2.402)	438.0 (2.416)	436.0 (2.406)	540	546	549	550	4312	4621	4880	5074
	287.0 (3.887)	286.0 (3.886)	280.0 (3.685)	278.0 (3.667)								
Dichloromethane	447.0 (2.373)	440.0 (2.307)	448.0 (2.425)	453.0 (2.438)	542	547	551	560	4806	5292	5173	5291
	274.0 (3.667)	275.0 (3.666)	276.0 (3.780)	277.0 (3.656)								
Ethyl acetate	370.0 (3.190)	376.0 (3.118)	381.0 (3.123)	383.0 (3.090)	552	555	560	562	4611	4505	4870	4985
	438.0 (2.416)	436.0 (2.398)	433.0 (2.543)	430.0 (2.232)								
1-Butanol	278.0 (3.720)	278.0 (3.974)	280.0 (3.706)	280.0 (3.691)	560	563	567	568	5345	5712	5511	5330
	376.0 (3.278)	380.0 (3.283)	377.0 (3.196)	370.0 (3.088)								
Ethanol	430.0 (2.323)	426.0 (2.422)	430.0 (2.308)	432.0 (2.334)	570	572	574	576	5930	5882	5834	5787
	276.0 (3.661)	277.0 (3.664)	278.0 (3.698)	279.0 (3.664)								
Methanol	440.0 (2.415)	444.0 (2.350)	440.0 (2.425)	439.0 (2.451)	578	580	582	581	5582	5907	6074	5936
	272.0 (3.750)	273.0 (3.730)	275.0 (3.875)	276.0 (3.868)								
Acetonitrile	387.0 (3.249)	382.0 (3.283)	386.0 (3.242)	385.0 (3.121)	582	583	585	588	5649	5995	5947	6035
	431.0 (2.516)	426.0 (2.562)	432.0 (2.309)	436.0 (2.432)								
Solid emission spectra	280.0 (2.651)	280.0 (3.741)	281.0 (3.869)	282.0 (3.674)	526	532	536	540				
	380.0 (3.276)	378.0 (3.164)	383.0 (3.244)	380.0 (3.185)								
	426.0 (3.417)	428.0 (2.479)	430.0 (2.218)	432.0 (2.447)								
	278.0 (3.873)	272.0 (3.857)	276.0 (3.872)	274.0 (3.650)								
	388.0 (3.192)	383.0 (3.171)	384.0 (3.126)	380.0 (3.185)								
	437.0 (2.410)	432.0 (2.636)	430.0 (2.140)	432.0 (2.247)								
	283.0 (3.694)	282.0 (3.668)	284.0 (3.657)	283.0 (3.622)								
	371.0 (3.308)	373.0 (3.179)	376.0 (3.082)	380.0 (3.087)								
	438.0 (2.240)	432.0 (2.407)	434.0 (2.536)	434.0 (2.244)								

^a UV–vis absorption measured in solution concentration = 1×10^{-5} M.

^b Photoluminescence measured in solution concentration = 1×10^{-4} M.

are almost similar to that of emission in non-polar solvent (*n*-hexane) which shows that there is very little or no influence of molecular interaction on the excited state of iridium complexes in the solid state [27]. Measurement of absorption solvatochromism has been interpreted with Marcus and Richardt–Dimroth solvent functions to estimate the transition dipoles associated with low lying MLCT excited state. The linear correlation (Fig. 6) of solvent shift of absorption band positions of iridium complexes **1–4** with Richardt–Dimroth solvent E_T parameters is indicative of the fact that the dielectric solute solvent interactions are responsible for the observed solvatochromic shift for the iridium complexes. The observed linear correlation (Fig. 5) of solvent shift of absorption band positions of iridium complexes **1–4** with Marcus [28] optical dielectric solvent function $[(1 - D_{op})/(2D_{op} + 1)]$ (Fig. 6) reveal that transition dipoles associated with absorption and the direction of excited dipole is opposite to that of the ground state-dipole (Fig. 7). Application of Marcus theory interpretation of solvent shift absorption data indicate that the absorption bands in the range 370–447 nm in these *ortho*-metalated Ir (III) complexes are due to MLCT transitions to the chelating ligand. Further linear correlation suggests as a result of the absorption that charge is transferred from the region around the *ortho*-metalated carbon atom to the region around the bridgehead of the chelating ligand and ground state dipole pointed toward the *ortho*-metalated carbon atom and an excited state dipole pointed toward the chelating ligand [28].

3.3. Electronic transition theory

The absolute PL quantum yields were measured by comparing fluorescence intensities (integrated areas) of a standard sample (Coumarin 46) and the unknown sample [18,21]. The main decay

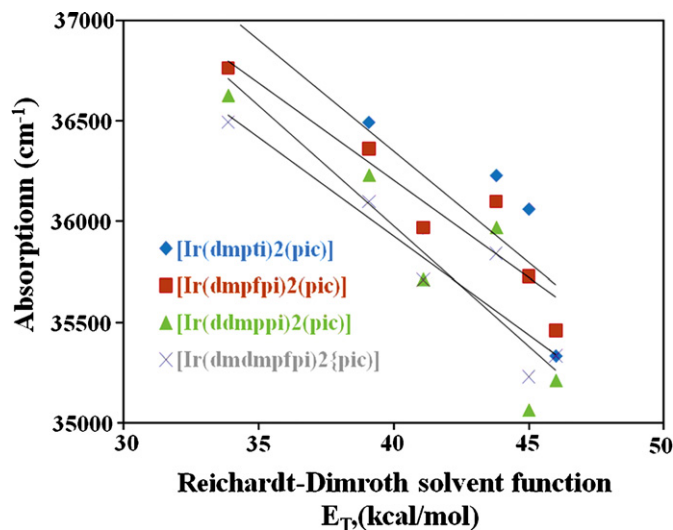


Fig. 5. Solvatochromic absorption of **1–4** with Richardt–Dimroth solvent E_T parameters.

route of the excited state of these complexes (**1–4**) and their radiative and non-radiative decay are studied in detail (Table 2). All these complexes (**1–4**) exhibit appreciable phosphorescence quantum yields at room temperature under nitrogen atmosphere. These values appear to be high for $(\text{fpdmdmpi})_2\text{Ir}(\text{pic})$ (**4**) complex [26]. Moreover, radiative lifetime of these complexes fall in the range of 1.1–2.4 μs . Among these complexes, a significant feature of the highly emitting iridium complex $(\text{fpdmdmpi})_2\text{Ir}(\text{pic})$ (**4**) has short triplet excited state lifetime of 1.1 μs .

Table 2
Photophysical properties of iridium complexes 1–4.

Complex	ϕ^a	τ (μs) 298 K	k_r (μs^{-1})	k_{nr} (μs^{-1})	HOMO ^b (eV)	LUMO ^c (eV)	E_g (eV)	E_{onset} (V)
1	0.30	2.4	0.13	0.29	−5.09	−2.20	2.89	0.21
2	0.35	2.0	0.17	0.33	−5.05	−2.40	2.65	0.25
3	0.41	1.7	0.22	0.36	−5.22	−2.83	2.39	0.42
4	0.46	1.1	0.42	0.49	−5.35	−3.34	2.01	0.55

Φ_{unk} is quantum yield of the sample, Φ_{std} is quantum yield of the standard; I_{unk} and I_{std} are the integrated emission intensities of the sample and the standard, respectively. A_{unk} , and A_{std} are the absorbances of the sample and the standard at the excitation wavelength, respectively. η_{unk} and η_{std} are the indexes of refraction of the sample and standard solutions.

$$^a \Phi_{\text{unk}} = \Phi_{\text{std}} \left(\frac{I_{\text{unk}}}{I_{\text{std}}} \right) \left(\frac{A_{\text{std}}}{A_{\text{unk}}} \right) \left(\frac{\eta_{\text{unk}}}{\eta_{\text{std}}} \right)^2$$

$$^b E_{\text{HOMO}} = 4.8 + E_{\text{(onset)}}$$

$$^c E_{\text{LUMO}} = E_{\text{HOMO}} - 1239/\lambda_{\text{abs}}$$

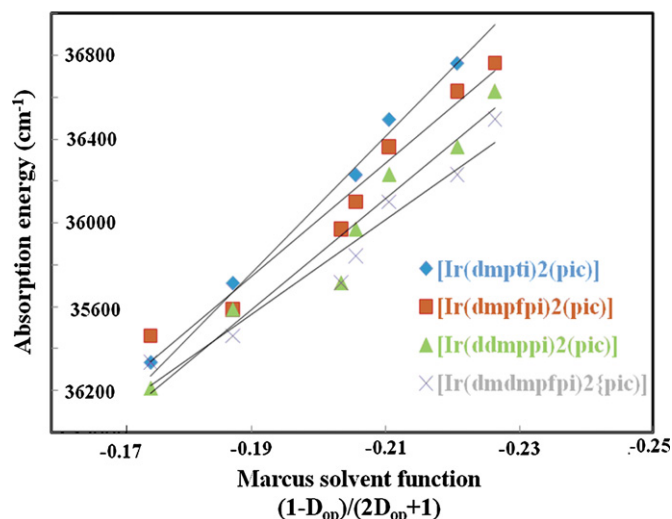


Fig. 6. Solvatochromic absorption of 1–4 with Marcus optical dielectric solvent function.

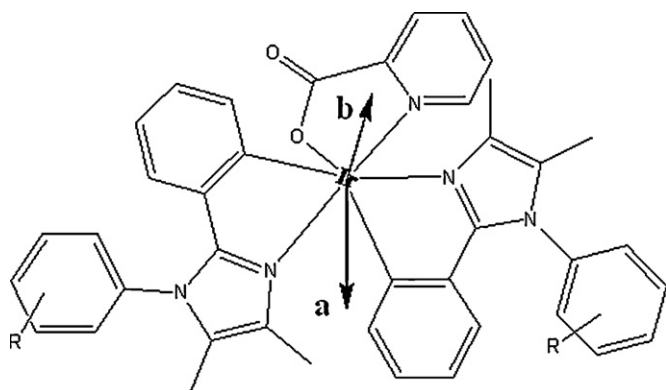


Fig. 7. Direction of ground state and excited state dipole moment in Iridium complex.

The radiative (k_r) and non-radiative (k_{nr}) rate constants (Fig. 8) are calculated from the phosphorescence yield Φ_p and lifetime τ ,

$$\Phi_p = \Phi_{\text{ISC}} \left\{ \frac{k_r}{k_r + k_{nr}} \right\} \quad (2)$$

$$\tau = (k_r + k_{nr})^{-1} \quad (3)$$

Here, Φ_{ISC} is the intersystem-crossing yield. For the iridium complexes Φ_{ISC} is safely assumed to be 1.0 because of the strong spin–orbit interaction caused by heavy atom effects of iridium [29]. k_r and k_{nr} are the radiative and non-radiative deactivation, τ_f is the life time of the S_1 excited state. The low quantum yields could be

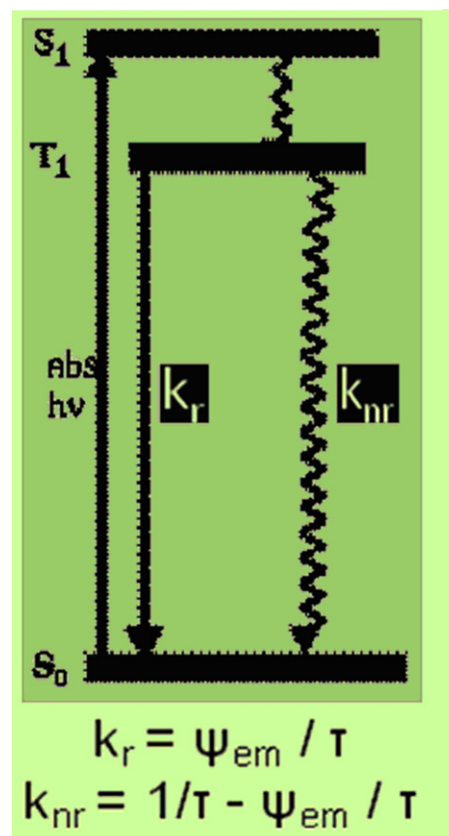


Fig. 8. Schematic representation of emission kinetics.

explained by non-radiative path to the low-lying $n-\pi^*$ state of the nitrogen atoms.

From the plot (Fig. 9a) of the phosphorescence yield (Φ) versus the maximum emission energy of phosphorescence (λ_{em}), it was found that the quantum yields range from 0.25 to 0.40 and roughly tend to increase with an increase in λ_{em} . Fig. 9b indicates that the k_r values of 1–4 increases with an increase of λ_{em} . According to the theory of the electronic transition, the k_r value is proportional to the square of the electric dipole transition moment (M_{T-S}). First-order perturbation theory gives an approximate expression for M_{T-S} [30]

$$M_{T-S} = \sum \beta_n <^1\Phi_n | \mathbf{M} | ^1\Phi_0 \quad (4)$$

where $^1\Phi_n$ and $^1\Phi_0$ are the wave functions of S_n and S_0 states, respectively and \mathbf{M} is the electric dipole vector with the use of the spin–orbit coupling operator (H_{so}) and the wave function of the

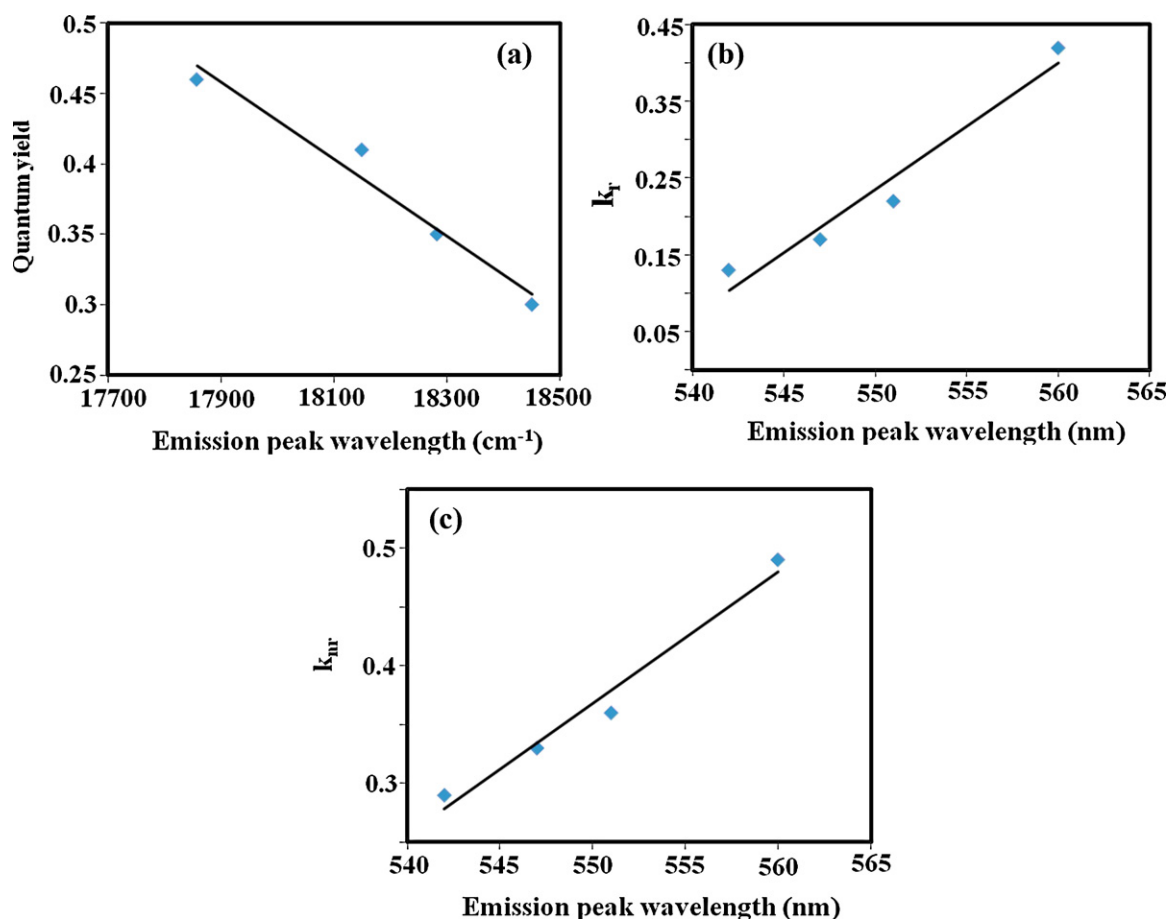


Fig. 9. (a) Plot of emission peak wavelength versus quantum yield. (b) Plot of emission peak wavelength versus k_r . (c) Plot of emission peak wavelength versus k_{nr} .

lowest excited triplet state ($^3\Phi_1$), β_n is formulated as

$$\beta_n = \langle ^1\Phi_n | H_{SO} | \frac{^3\Phi_1}{(^1E_n - ^3E_1)} \rangle \quad (5)$$

where 1E_n and 3E_1 are the energies of S_n state and the lowest excited triplet state, respectively. Now, Eq. (4) is simply expressed as

$$M_{T-S} = \frac{\langle ^1\Phi_n | H_{SO} | ^3\Phi_1 \rangle \langle ^1\Phi_1 | M | ^1\Phi_0 \rangle}{\alpha ({}^1E_1 - {}^3E_1)} \quad (6)$$

$$= \frac{\alpha}{({}^1E_1 - {}^3E_1)}$$

Eq. (6) predicts that, when $\alpha = \langle ^1\Phi_n | H_{SO} | ^3\Phi_1 \rangle \langle ^1\Phi_1 | M | ^1\Phi_0 \rangle$ is approximately constant, Since M_{T-S} k_r increases with a decrease in the energy difference (${}^1E_1 - {}^3E_1$), k_r also increases with a decrease in the energy difference (Table 2). In the present study, k_r and k_{nr} increases with an increase in λ_{em} (Fig. 9b and c). This fact is explained by assuming that the S_1 energy does not differ significantly among the complexes **1–4** and the energy difference (${}^1E_1 - {}^3E_1$), increases with decrease in λ_{em} . Actually in complexes **1–4**, the $S_1 \leftarrow S_0$ absorption bands are located at 426–432 nm. But phosphorescence $S_0 \leftarrow T_1$ exhibits large bathochromic shift ranging from 528 to 588 nm. These data (Fig. 9b) provide the evidence that the energy difference (${}^1E_1 - {}^3E_1$), increases with the decrease in λ_{em} and therefore, k_r increases with an increase in λ_{em} [30].

3.4. Energy gap law vs drop in k_{nr} – potential energy surface diagram

It has been found that the behaviour of most transition metal systems can be accommodated by the energy gap law [30–33].

The physical construct of multiphonon nonadiabatic description of electron transfer developed by Freed and Jortner [34], Englman and Jortner [35] and Jortner [36] describes, the relation between a non-radiative transition k_{nr} and the energy gap (E_g) is given in Eq. (7) [31].

$$k_{nr} \propto \exp\left(\frac{-\gamma E_g}{\hbar\omega_M}\right) \quad \gamma = \ln\left(\frac{E_g}{S_M \hbar\omega_M}\right) - 1 \quad (7)$$

where the energy gap (E_g) is related to the zero-point energy (ZPE) separations of two coupled surfaces. The $\hbar\omega_M$ term describes, in the limit of a single configuration co-ordinates model, the average energy of the vibrational model that couples the final state of the initial state. The degree to which the two surfaces are vibronically coupled is gauged by the Huang–Rhys factor (S_M),

$$S_M = \frac{1}{2} \left(\frac{M\omega_M}{\hbar}\right) (\Delta Q_e)^2 \quad (8)$$

where M is the reduced mass of the oscillator, ω_M is the fundamental frequency and ω_M represents the difference between the ground- and excited-state equilibrium geometries with respect to the specified nuclear (i.e., vibrational) coordinate. The changes in both E_0 and ΔQ_e have effect on vibrational overlap k_{nr} is shown pictorially in Fig. 10. On comparison with the central potential energy surface diagram (B), a decrease in the energy gap at constant ΔQ_e (C) results in an increase in the vibrational overlap between the excited state and ground states surfaces. Conversely, increasing the energy gap has the opposite effect, i.e., decrease in vibrational overlap leading to a smaller value for k_{nr} [energy gap law (Fig. 11a)]. With a larger ΔQ_e (A), favouring vibrational overlap and leading to a larger value for k_{nr} .

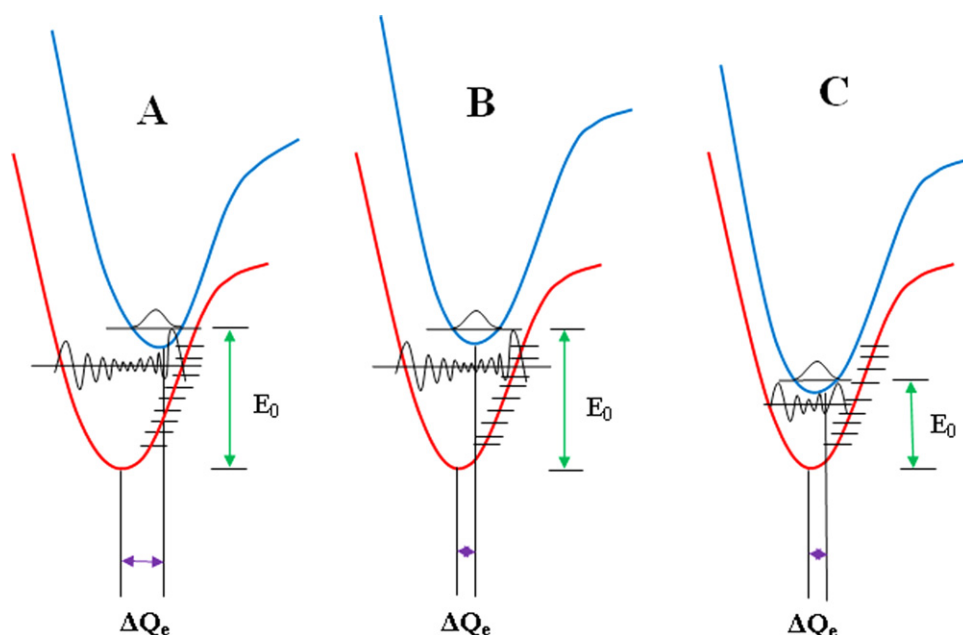


Fig. 10. Graphical illustration of the factors influencing vibrational overlap for non-radiative excited state decay.

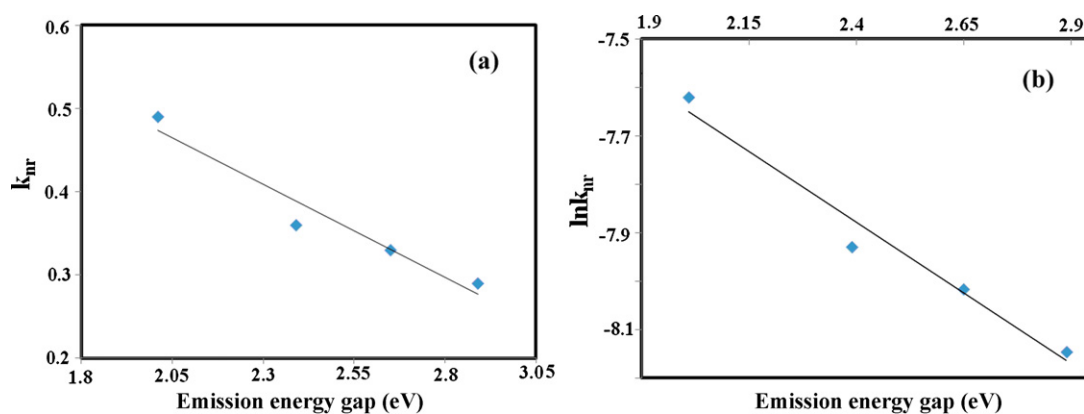


Fig. 11. (a) Plot of k_{nr} versus emission energy gap. (b) Plot of $\ln(k_{nr})$ versus emission energy gap.

The plot of $\ln(k_{nr})$ versus energy gap for complexes 1–4 (Fig. 11b) shows that there is good qualitative agreement with the “Energy gap law”. The Energy gap law predicts that the rate of non-radiative decay increases when the energy gap separating the ground and excited state decreases. The relation is based on the vibrational overlap between the ground state and the excited state, k_{nr} is a function of Franck–Condon overlap integral. These complexes having similar excited states and vibrational coupling, a simplified form of the energy gap law is obtained that predicts a linear correlation between $\ln(k_{nr})$ and the energy gap [14]. The slope of -0.59 eV^{-1} is similar in magnitude to those found for iridium(III) complexes [26] which have the $^3\text{MLCT}$ excited states for the lowest excited triplet states. This correlation suggests that the change of non-radiative decay rate constant is owing to the energy gap of the complexes [37].

3.5. Effect of substituents on tuning wavelength

Substituent effect of the d orbital (t_{2g}) stabilization of iridium metal through the carbon atom-iridium bonding and this identifies with the inductive effect of the substituents. Therefore, the HOMO stability and the emission energy gap are controlled by the nature and number of substituents and its inductive influence

on the aromatic ring. The photophysical study of these complexes demonstrates that the electron releasing substituent increases the absorption and emission energies of complexes by stabilizing the HOMO level. Besides increasing the emission energy, the lower HOMO energies decrease the energy separation between the $^1\text{MLCT}$ and ^3LC states, which in turn modified the excited state properties of the iridium complexes.

The redox potentials of the cyclometalated iridium complexes were measured relative to an internal ferrocene reference ($\text{Cp}_2\text{Fe}/\text{Cp}_2\text{Fe}^+ = 0.45 \text{ V}$ versus SCE in CH_2Cl_2 solvent) [38,39]. As revealed previously [40,41], the reductions occur primarily on the more electron accepting heterocyclic portion of the cyclometalated 2-arylimidazole ligands (LUMO contribution) whereas the oxidation process is to largely involved in the Ir-phenyl center (HOMO contribution). The calculated energies of the highest occupied molecular orbital (HOMO) and lowest unoccupied molecular orbital (LUMO) are given in Table 2.

The iridium complexes show reversible oxidation behaviour and these complexes exhibit HOMO levels ranging of 5.09–5.35 eV. The LUMO energies were calculated based on the HOMO energies and the lowest-energy absorption edges of the UV–vis absorption spectra [39] (Fig. 12). These results reveal that the mono-methyl substituted complexes 1 and 2 show emission with the shorter

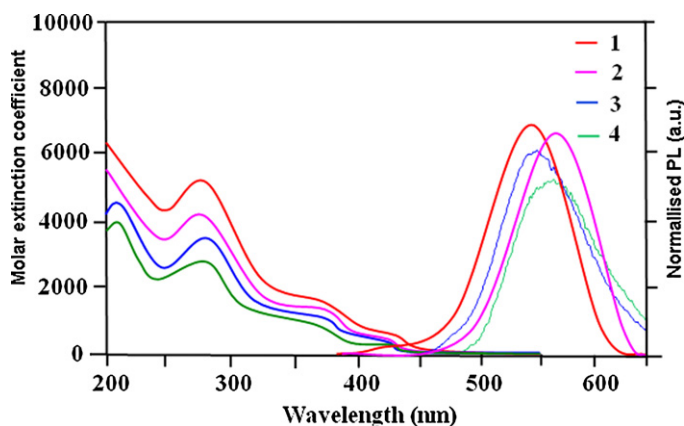


Fig. 12. Normalized sigma plot of absorption and emission of 1–4 in CH_2Cl_2 .



Fig. 13. Solution color of the photoluminescence for complexes 2 and 4 in CH_2Cl_2 .

wavelength [542 (1) and 550 (2)] (maximum E_g) whereas dimethyl substituted complexes [Ir(dmdmp)2(pic) (3) and Ir(fpdm)2(pic) (4)] (minimum E_g) exhibit emission with maximum wavelength [553 (3) and 560 nm (4)] in dichloromethane. From the energy gap values it was concluded that all the reported dopants (1–4) are green emitters (Fig. 13).

4. Conclusions

In summary we introduced novel green emitting Ir(III) complex dopants using various substituted imidazole ligands. These complexes exhibit different quantum efficiencies in solution depending upon the nature of substituents. The observed results show that the wavelength can be tuned to greater extent depending upon the substituents in the ligand. Some of the complexes discussed here showed $^3\text{MLCT}$ predominant mixing states for their lowest excited triplet states, but the degree of mixing between $^3\text{MLCT}$ and $^3\pi-\pi^*$

states of the excited states varied. The solvent shifts are interpreted in terms of Richardt–Dimroth and Marcus solvent functions. The results consistent with prior assignments on the absorption band to a metal-to-ligand charge transfer excited state associated with chelating ligand. Electronic transition theory is applied to study the effect of E_g and ΔQ_e on non-radiative transition (k_{nr}). With a larger ΔQ_e , favouring vibrational overlap and leading to a larger value for k_{nr} . Effort toward the development of RGB color complexes using different substituents are currently underway and investigation of device studies for these iridium complexes are also currently in progress.

Acknowledgements

One of the authors Dr. J. Jayabharathi, Associate Professor, Department of Chemistry, Annamalai University is thankful to Department of Science and Technology [No. SR/S1/IC-07/2007] and University Grants Commission (F. No. 36-21/2008 (SR)) for providing funds to this research work and Prof. C.H. Cheng, Chairman, National Science Council, National Tsing Hua University, Taiwan, ROC for my post-doctoral research work.

References

- [1] M.A. Baldo, D.F. O'Brien, Y. You, A. Shoustikov, M.E. Thompson, S.R. Forrest, *Nature* 395 (1988) 151–154.
- [2] M.A. Baldo, M.E. Thompson, S.R. Forrest, *Pure Appl. Chem.* 71 (1999) 2095–2106.
- [3] C.X. Li, G.H. Zhang, H.H. Shih, X. Jiang, P.P. Sun, C.H. Cheng, *J. Organomet. Chem.* 694 (2009) 2415–2420.
- [4] P.P. Sun, J.P. Duan, J.J. Lih, C.H. Cheng, *Adv. Funct. Mater.* 13 (2003) 683–691.
- [5] Y.L. Tung, S.W. Lee, Y. Chi, Y.T. Tao, C.H. Chien, Y.M. Cheng, P.T. Chou, S.M. Peng, C.S. Liu, *J. Mater. Chem.* 15 (2005) 460.
- [6] H. Xia, Y.Y. Zhu, D. Lu, M. Li, C.B. Zhang, B. Yang, Y.G. Ma, *J. Phys. Chem. B* 110 (2006) 18718–18723.
- [7] Y.J. Su, H.L. Huang, C.L. Li, C.H. Chien, Y.T. Tao, P.T. Chou, S. Datta, R.S. Liu, *Adv. Mater.* 15 (2003) 884–888.
- [8] T. Tsuzuki, S. Tokito, *Adv. Mater.* 19 (2007) 276–280.
- [9] D.K. Rayabarapu, B.M.J.S. Paulose, J.P. Duan, C.H. Cheng, *Adv. Mater.* 17 (2005) 349.
- [10] I. Avilov, P. Minoofar, J. Cornil, L.D. Cola, *J. Am. Chem. Soc.* 129 (2007) 8247.
- [11] E.M. Hwang, H.Y. Chen, P.S. Chen, C.S. Liu, C.F. Shu, E.L. Wu, P.T. Chou, S.M. Peng, G.H. Lee, *Inorg. Chem.* 44 (2005) 1344–1353.
- [12] S. Lamansky, P. Djurovich, D. Murphy, F. Abdel-Razzaq, H.F. Lee, C. Adachi, P.E. Burrows, S.R. Forrest, M.E. Thompson, *J. Am. Chem. Soc.* 123 (2001) 4304–4312.
- [13] M.E. Thompson, S. Lamansky, P. Djurovich, D. Murphy, F. Abdel-Razzaq, R. Kwong, S.R. Forrest, M.A. Baldo, P.E. Burrows, US Patent 20020034656A1.
- [14] K. Brooks, Y. Babayan, S. Lamansky, P.I. Djurovich, I. Tsyba, R. Bau, M.E. Thompson, *Inorg. Chem.* 41 (2002) 3055–3066.
- [15] V.V. Grushin, N. Herron, D.D. LeCloux, W.J. Marshall, V.A. Petrov, Y. Wang, *Chem. Commun.* 16 (2001) 1494–1495.
- [16] W.C. Chang, A.T. Hu, J.P. Duan, D.K. Rayabarapu, C.H. Cheng, *J. Organomet. Chem.* 689 (2004) 4882–4888.
- [17] M.G. Colombo, A. Hauser, H.U. Gudel, *Inorg. Chem.* 32 (1993) 3088–3092.
- [18] J. Jayabharathi, V. Thanikachalam, K. Saravanan, N. Srinivasan, *J. Fluoresc.* (2010), doi:10.1007/s10895-010-0737-7.
- [19] K. Saravanan, N. Srinivasan, V. Thanikachalam, J. Jayabharathi, *J. Fluoresc.* (2010), doi:10.1007/s10895-010-0690-5.
- [20] J. Jayabharathi, V. Thanikachalam, N. Srinivasan, K. Saravanan, *J. Fluoresc.* (2010), doi:10.1007/s10895-010-0747-5.
- [21] J. Jayabharathi, V. Thanikachalam, K. Saravanan, *J. Photochem. Photobiol. A* 208 (2009) 13–20.
- [22] M. Nonoyama, *Bull. Chem. Soc. Jpn.* 47 (1974) 767–768.
- [23] S. Lamansky, P. Djurovich, D. Murphy, F. Abdel-Razzaq, R. Kwong, I. Tsyba, M. Bortz, B. Mui, R. Bau, M.E. Thompson, *Inorg. Chem.* 40 (2001) 1704–1711.
- [24] B.X. Mi, P.F. Wang, M.W. Liu, H.L. Kwong, N.B. Wong, C.S. Lee, S.T. Lee, *Chem. Mater.* 15 (2003) 3148–3151.
- [25] J. DePriest, G.Y. Zheng, N. Goswami, D.M. Eichhorn, C. Woods, D.P. Rillema, *Inorg. Chem.* 39 (2000) 1955–1963.
- [26] S. Okada, K. Okinaka, H. Iwawaki, M. Furugori, M. Hashimoto, T. Mukaide, J. Kamatani, S. Igawa, A. Tsuboyama, T. Takiguchi, K. Ueno, *Dalton Trans.* 9 (2005) 1583–1590.
- [27] J. Lundin, A.G. Blackman, K.C. Gordon, D.L. Officer, *Angew. Chem. Int. Ed.* 45 (2006) 2582–2584.
- [28] A.P. Wilde, R.J. Watts, *J. Phys. Chem.* 95 (1991) 622–629.
- [29] S.D. Cummings, R. Eisenberg, *J. Am. Chem. Soc.* 118 (1996) 1949–1960.
- [30] J.B. Bricks, *Photophysics of Aromatic Molecules*, Wiley-Interscience, London, 1970.

- [31] J.A. Treadway, B. Loeb, R. Lopez, P.A. Anderson, F.R. Keene, T.J. Meyer, *Inorg. Chem.* 35 (1996) 2242–2246.
- [32] K.R. Barqawi, Z. Murtaza, T.J. Meyer, *J. Phys. Chem.* 95 (1991) 47–50.
- [33] J.V. Casper, T.J. Meyer, *J. Phys. Chem.* 87 (1983) 952–957.
- [34] K.F. Freed, J. Jortner, *J. Chem. Phys.* 52 (1970) 6272–6291.
- [35] R. Englman, J. Jortner, *J. Mol. Phys.* 18 (1970) 145–164.
- [36] J. Jortner, *J. Chem. Phys.* 64 (1976) 4860–4867.
- [37] N.H. Damrauer, T.R. Bousie, M. Devenney, J.K. McCusker, *J. Am. Chem. Soc.* 119 (1997) 8253–8268.
- [38] R.R. Gange, C.A. Koval, G.C. Lisensky, *Inorg. Chem.* 19 (1980) 2854–2855.
- [39] S. Ranjan, S.Y. Lin, K.C. Hwang, Y. Chi, W.L. Ching, C.S. Liu, Y.T. Tao, C.H. Chien, S.M. Peng, G.H. Lee, *Inorg. Chem.* 42 (2003) 1248–1255.
- [40] P.J. Hay, *J. Phys. Chem. A* 106 (2002) 1634–1641.
- [41] M. Sudhakar, P.I. Djurovich, Hogen-T.E. Esch, M.E. Thompson, *J. Am. Chem. Soc.* 125 (2003) 7796–7797.